RSC Advances

PAPER

View Article Online
View Journal | View Issue



Cite this: *RSC Adv.*, 2022, **12**, 33716

# Bimetal NiCo-MOF-74 for highly selective NO capture from flue gas under ambient conditions†

Jie Hu,‡[a] Lei Li,‡[a] Hao Li,[a] Ying Zhai,[a] Fushun Tang,*[a] Zhe Zhang[a] and Banglin Chen *[b]

Received 21st September 2022
Accepted 18th November 2022

DOI: 10.1039/d2ra05974f

rsc.li/rsc-advances

The mixed bimetal metal–organic framework $Ni_{0.37}Co_{0.63}$-MOF-74 has been constructed by the solvothermal method for NO adsorption. The results showed that bimetal $Ni_{0.37}Co_{0.63}$-MOF-74 takes up NO with a capacity of up to 174.3 cc $g^{-1}$ under ambient conditions, which is 16.3% higher than that of the best single metal Co-MOF-74. The IAST adsorption selectivity for a NO/$CO_2$ binary mixture can reach a maximum of 710 at low adsorption partial pressure, while the regeneration performance can be retained even after five cyclic adsorption–desorption experiments. Its separation performance was further confirmed by breakthrough experiments, indicating this new bimetal $Ni_{0.37}Co_{0.63}$-MOF-74 as one of the best materials for NO adsorption and separation in flue gas.

## Introduction

Nitrogen oxides cause environmental problems such as photochemical smog, acid rain, ozone layer destruction and the greenhouse effect, and are considered to be one of the major air pollutants.[1] At present, the more mature nitrogen oxide purification technology is catalytic reduction, but it faces some problems such as catalyst poisoning and low removal efficiency of low concentration $NO_x$.[2] Using an adsorbent to treat flue gas can cause low concentration $NO_x$ to adsorb directly and then, through the heating or decompression method, to be released, so as to allow the adsorbent to be recycled and reused. In order to realize the efficient adsorption of nitrogen oxides, a kind of adsorbent with good selectivity, large adsorption capacity and good regeneration performance is needed first.[3]

Metal–organic framework material (MOFs) is a kind of material with periodic grid structure, which is assembled by metal ions and organic ligands. It has the advantages of high specific surface area, large porosity, diversified and adjustable pore structure, so it has been widely studied and applied.[4–6] M-MOF-74 (M = Mg, Co, Ni, Zn, Mn, Fe) series materials are composed of divalent metal ions and 2,5-dihydroxyterephthalic acid (DOBDC) organic ligands, and have a three-dimensional honeycomb structure with a large number of open metal sites in the pores, which have been widely studied in the field of gas adsorption separation and show excellent gas adsorption and separation properties.[7–11] The unique secondary structural unit of MOF-74 has stronger fault tolerance to polymetals,[12] so it is an ideal object for the study of polymetallic MOFs materials.[13]

Unsaturated metal sites play a key role in the adsorption and release of NO, while M-MIL-53 without unsaturated metal sites is weaker in NO adsorption.[14] Both Co-CPO-27 and Ni-CPO-27 of single metal nodes show a well NO adsorption capacity at unsaturated metal sites, and almost all adsorbed NO can be released by triggering with water molecules.[15] MOF-74 materials containing ZnCo[16] and MgNi[17] bimetallic sites can also improve the storage and release properties of NO. Although their performance for the storage and release of pure medical NO has been examined; their potentials for the adsorption and separation of NO in flue gas mixture have not been explored yet.

The polymetallic site MOF-74 with expected topology can be synthesized by introducing different metal nodes, which can bring unique adsorption properties.[18] In this paper, Ni and Co metals were assembled on MOF-74 structure by solvothermal method, the selective adsorption and separation performance of bimetal NiCo-MOF-74 for NO in gas mixture was examined. The resulting $Ni_{0.37}Co_{0.63}$-MOF-74 takes up large amount of NO of 174.3 cc $g^{-1}$ under ambient conditions, which is 16.3% higher than that of the best single metal Co-MOF-74. The IAST adsorption selectivity for NO/$CO_2$ binary mixture can reach a maximum of 710 at low adsorption partial pressure, while the regeneration performance can retain even after five cyclic adsorption–desorption experiments. Its separation performance was further confirmed by breakthrough experiments, indicating this new bimetal $Ni_{0.37}Co_{0.63}$-MOF-74 as one of the best materials for NO adsorption and separation in flue gas.

[a]*College of Chemistry and Bioengineering, Guilin University of Technology, Guilin 541004, China. E-mail: tfushun@163.com*

[b]*Department of Chemistry, The University of Texas at San Antonio, Texas 78249, USA. E-mail: banglin.chen@utsa.edu*

† Electronic supplementary information (ESI) available. See DOI: https://doi.org/10.1039/d2ra05974f

‡ These authors contributed equally to this work as co-first authors.

# Experimental

### Materials and chemicals

Cobalt nitrate hexahydrate ($Co(NO_3)_2 \cdot 6H_2O$, AR, Aladdin Co.); nickel nitrate hexahydrate ($Ni(NO_3)_2 \cdot 6H_2O$, AR, Aladdin Co.); 2,5-dihydroxyterephthalic acid (DOBDC, AR, Aladdin Co.); *N*,*N*-dimethylformamide (DMF, AR, Aladdin Co.); ethanol ($C_2H_5OH$, AR, Rhawn Co.); methanol ($CH_3OH$, AR, Rhawn Co.).

### Material preparation

MOF-74 was synthesized by solvothermal method and adjusted appropriately during the experiment.[19]

### Synthesis of Co-MOF-74

1.2 g (4.12 mmol) cobalt nitrate hexahydrate ($Co(NO_3)_2 \cdot 6H_2O$, AR), 0.272 g (1.37 mmol) and 2,5-dihydroxyterephthalic acid (DOBDC, AR) were dissolved in 60 mL mixed solution of *N*,*N*-dimethylformamide (DMF), absolute ethanol and deionized water with volume ratio 15 : 1 : 1. After stirring for 30 minutes, the synthesized solution was transferred to the Teflon-lined reactor, placed in a 393 K oven for 72 h, then cooled to room temperature. The product was washed with DMF three times, and purified with methanol for 6 d (changing the solution every 12 h), and then put into a 473 K vacuum drying oven to dry for 8 h after filtering.

### Synthesis of Ni-MOF-74

The synthesis method is mostly the same as Co-MOF-74 while the $Co(NO_3)_2 \cdot 6H_2O$ was replaced with $Ni(NO_3)_2 \cdot 6H_2O$.

### Synthesis of NiCo-MOF-74

The bimetal material NiCo-MOF-74 was synthesized using the same method as above. With keeping the total amount of metal ions constant, the molar fractions of total metal ions in the synthesized solution for $Ni^{2+}$ and $Co^{2+}$ were 0.4 and 0.6, respectively. NiCo-MOF-74 was prepared for component analysis by ICP, the results showed that the contents of Ni and Co were 9.88 wt% and 16.96 wt%, respectively, so the actual molar ratio of Ni to Co was around 0.37 : 0.63, and the bimetal material NiCo-MOF-74 was expressed as $Ni_{0.37}Co_{0.63}$-MOF-74 rather than the feed ratio.

### Characterization analysis

Quantitative Analysis of Ni and Co in samples by Inductively coupled Plasma Atomic Emission Spectrometry (ICP, Aglient 720ES), the preparation of the solution to be tested was as follows. About 0.0387 g weighed sample for analysis was placed in a Teflon crucible, then a certain concentration of digestion solution consisting of hydrochloric acid and nitric acid was added to the sample for digestion. After that, the sample was cooled and transferred to a volumetric flask and then diluted with pure water to 10 mL to obtain the solution to be measured. Since each element had characteristic spectral lines that were not interfered by other elements, the instrument can test multiple elements simultaneously on the sample to be measured.

Powder X-ray Diffraction (PXRD) patterns were obtained on a Panaco Netherlands using Cu ($\lambda$ = 154 056 Å); the SEM morphology of the samples was characterized by a thermoelectric field emission scanning electron microscope (SU 5000); thermogravimetric analysis (TG) was carried out under $N_2$ atmosphere from room temperature to 600 °C using a Netzsch SPA-500 thermogravimetric analyzer at a heating rate of 10 °C $min^{-1}$; NO adsorption *in situ* diffuse reflectance infrared spectroscopy (DRIFTS) was carried out on Thermo-Scientific IS10 FTIR spectrometer with a scan range of 4000–400 $cm^{-1}$ at 298 K, the samples were first pretreated at 373 K, the IR spectra of the pretreated samples in $N_2$ atmosphere were used as the background, and then the *in situ* IR spectra of the samples after NO adsorption were collected; the samples specific surface area and pore size structure were determined by SSA-7000 physical adsorption instrument (Beijing Builder Co., China).

### Material performance test

SSA-7000 physical adsorption instrument (Beijing builder Co., CN) was used to test the isothermal adsorption performance of materials (NO, $CO_2$, $N_2$) by the static method under 298 K and 0–100 kPa conditions.

The adsorption selectivity of the materials in simulated flue gases was studied using a DECRA (Hiden Co., UK) quantitative gas analysis mass spectrometer and the gas mixture of 20 mL $min^{-1}$ was controlled by mass flow meter (contained 2000 ppm $CO_2$, 1000 ppm NO, $N_2$ remainder). The process was as follows: putting 0.01 g of sample in the reaction tube, using nitrogen to the clean of gas path; waiting for the instrument signal to stabilize, switching the valve to pass the gas mixture into the reaction tube; after the sample adsorption reaches equilibrium, the instrument signal was stable.

Assuming that the time of $N_2$ passing through the empty tube is constant at the same flow rate, the adsorption amount of a unit mass sample in the mixed gas component is calculated by using eqn (1):

$$N = \frac{v \times S_i}{m} \quad (1)$$

where, $v$ was the flow rate of the mixed gas, $S_i$ was the peak area of the adsorption curve of gas i, and $m$ was the mass of the sample.

# Results and discussion

### Structure and thermal stability of the synthesized products

Fig. 1 showed the PXRD spectra of Co-MOF-74, Ni-MOF-74 and $Ni_{0.37}Co_{0.63}$-MOF-74.

It can be seen that there were obvious diffraction peaks at $2\theta$ = 6.74° and 11.7° on Co-MOF-74, which was consistent with the PXRD spectra simulated by cif crystal structure data reported in the literature. And obvious diffraction peaks at $2\theta$ = 6.9° and 12° can be observed on Ni-MOF-74, they were slightly bigger than Co-MOF-74, which was consistent with the larger average

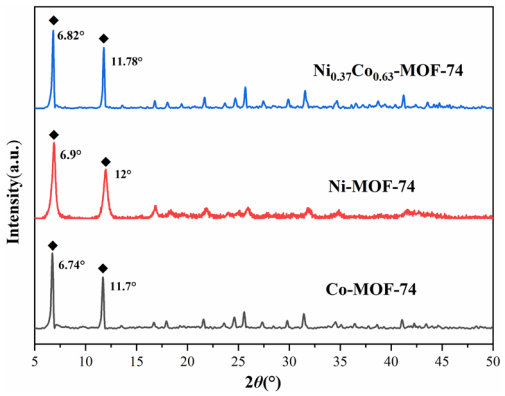


Fig. 1 PXRD spectra of Co-MOF-74, Ni-MOF-74 and $Ni_{0.37}Co_{0.63}$-MOF-74.

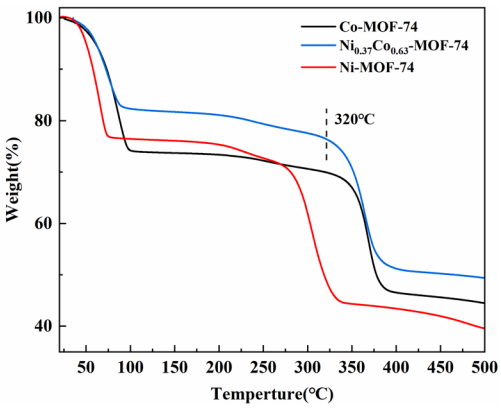


Fig. 2 TG curve of Co-MOF-74, Ni-MOF-74 and $Ni_{0.37}Co_{0.63}$-MOF-74.

aperture of Ni-MOF-74. However, the diffraction peak position of $Ni_{0.37}Co_{0.63}$-MOF-74 with smaller average pore aperture was slightly bigger than that of Co-MOF-74. Combined with the data of BET surface area and pore volume (seen in Table 1), it can be explained by that there were more micropores in the material of NiCo-MOF-74. In general, the bimetal MOFs had the same crystal structure as the single metal Co-MOF-74 material, and the synthesized product was MOF-74 structure.

Fig. 2 showed the thermal stability analysis (TG) of samples Co-MOF-74, Ni-MOF-74 and $Ni_{0.37}Co_{0.63}$-MOF-74. The weight loss trend of bimetal $Ni_{0.37}Co_{0.63}$-MOF-74 materials was basically the same as that of Co-MOF-74. In the first stage, the mass of the sample decreased rapidly with the increase of temperature, which was the removal of adsorption solvent and residual DMF on the sample surface. In the second stage, the mass of the sample decreased slowly during the subsequent heating process, mainly due to the removal of solvent and DMF in the pore, and the active site was exposed. In the third stage, when the temperature was above 320 °C, the weight of sample continued to lose 20%, which was presumed to be caused by the collapse of the sample structure, and the sample decomposes and loses activity. It can also be seen that Ni-MOF-74 began to show a large weight loss rate above 280 °C, which was lower than that of bimetal $Ni_{0.37}Co_{0.63}$-MOF-74 at 320 °C. The TG results showed that the pretreatment temperature should be about 200 °C for the exposure of metal sites to improve the adsorption properties of NO. At the same time, the thermal stability of bimetal $Ni_{0.37}Co_{0.63}$-MOF-74 was similar to that of Co-MOF-74 and had high thermal stability, so it should be suitable for use in flue gas surroundings.

Table 1 Structure parameters of Co-MOF-74, Ni-MOF-74 and $Ni_{0.37}Co_{0.63}$-MOF-74

| Sample | BET surface area ($m^2\ g^{-1}$) | Microporous volume ($cm^3\ g^{-1}$) | Average pore diameter (nm) |
|---|---|---|---|
| Co-MOF-74 | 928 | 0.458 | 2.3 |
| $Ni_{0.37}Co_{0.63}$-MOF-74 | 1019 | 0.502 | 2.28 |
| Ni-MOF-74 | 970 | 0.476 | 2.4 |

## Analysis of physical properties and structure

It was difficult to determine whether the synthetic material was bimetal coexisting in the same frame structure or the mixture of two kinds of isomorphic single metal MOF-74 (Co-MOF-74, Ni-MOF-74) by PXRD, so the morphology and metal element distribution of the samples were necessary to further explained by SEM and EDS. Fig. 3 showed the SEM images of Co-MOF-74 and $Ni_{0.37}Co_{0.63}$-MOF-74. As can be seen from the figure that the shape of Ni-MOF-74 was spindle shape and bulk stacking, while the shape of bimetal $Ni_{0.37}Co_{0.63}$-MOF-74 was similar to that of Co-MOF-74 as slender rod-like crystals. Metal centers have an important influence on the growth process of MOFs materials, the existence of bimetal centers will change the crystal growth process, resulting in small changes in crystal morphology and size.[20]

The growth process of MOF-74 materials also followed this law. The single crystal was selected for EDS analysis, and the distributive mapping in the $Ni_{0.37}Co_{0.63}$-MOF-74 crystal was observed as shown in Fig. 4. It can be seen that the two metal elements Ni and Co were uniformly distributed in the crystal, indicating that the synthesis of bimetal MOF-74 was not a simple physical mixture, Co and Ni can be uniformly assembled on the structural unit of MOF-74. Furthermore, the contents of Co and Ni determined by ICP were 16.96 wt% and 9.88 wt%, the molar ratio of Co to Ni were 0.631 and 0.370. It was close to the feed ratio of 0.6 to 0.4, indicating that the metal sites in the synthesized products can basically grow according to the feed ratio. Of course, in the synthesis of polymetallic MOFs materials, the molar ratio of the metal center in the

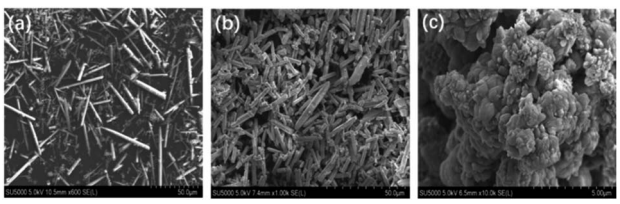


Fig. 3 SEM morphology of Co-MOF-74 (a), $Ni_{0.37}Co_{0.63}$-MOF-74 (b) and Ni-MOF-74 (c).

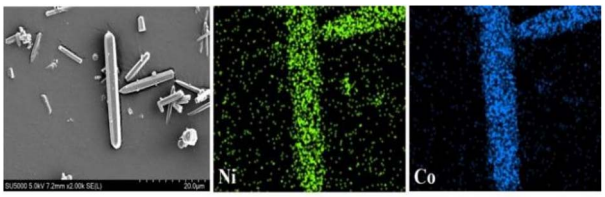


Fig. 4 The metal element mapping distribution map (EDS) of $Ni_{0.37}Co_{0.63}$-MOF-74.

products was not exactly the same as the feed ratio sometimes,[21] because the coordination reaction rate between different metal ions and ligands was different in the process of crystal growth.

Fig. S1† showed the $N_2$ adsorption isotherms of Co-MOF-74, Ni-MOF-74 and $Ni_{0.37}Co_{0.63}$-MOF-74 at 77 K. The $N_2$ adsorption isotherms of all tested materials were typical microporous type I curves, indicating that there was no big change in the structure of the bimetal materials after the introduction of Ni.

Considering that Ni and Co had similar atomic mass and their influence on the material structure should be negligible, so, in the case of the almost same pore size (shown in Table 1), the increase of specific surface area of $Ni_{0.37}Co_{0.63}$-MOF-74 may be caused by that the difference in the radius of $Ni^{2+}$ and $Co^{2+}$ metal ions and the different binding rate between metal elements and organic ligands affected the crystal growth process,[22] resulting in that there were some defects in the crystal (such as the absence of partial metals or ligands, or the existence of local mesoporous) during the construction of the structural unit, then led to the increase of the specific surface area of the sample. More details of pore distribution can be seen in Fig. S2,† there were more micropores in the material of NiCo-MOF-74, so their surface area and porous volume were also increased.

### Adsorption and separation performance

The adsorption of single component NO, $CO_2$ and $N_2$ by Co-MOF-74, Ni-MOF-74 and $Ni_{0.37}Co_{0.63}$-MOF-74 were tested using the static method at 298 K and 0–100 kPa, and the adsorption isotherms were shown in Fig. 5.

Considering the NO adsorption capacity of the three material, the results showed that the NO adsorption capacity of bimetal $Ni_{0.37}Co_{0.63}$-MOF-74 was higher than that of monometallic MOF-74. In the case of 100 kPa, the NO adsorption capacity of $Ni_{0.37}Co_{0.63}$-MOF-74 reached 174.3 cc $g^{-1}$, which was 16.4% and 6.1% higher than the 149.8 cc $g^{-1}$ adsorption capacity of Co-MOF-74 and 164.4 cc $g^{-1}$ adsorption capacity of Ni-MOF-74, respectively. The quick adsorption of NO was observed under lower pressure, indicating a better adsorption interaction between the metal framework and NO molecules. This may be due to the introduction of second metal sites in the MOF-74 skeleton. In addition, a sharp adsorption of NO was observed under lower pressure region, this indicated a better adsorption interaction between the metal framework and NO molecules which improved the NO adsorption performance of the material.

Considering the selectivity of these three materials, the adsorption characteristics of $Ni_{0.37}Co_{0.63}$-MOF-74 for NO, $CO_2$ and $N_2$ were similar to those of Co-MOF-74 and Ni-MOF-74. As same as Co-MOF-74 and Ni-MOF-74, $Ni_{0.37}Co_{0.63}$-MOF-74 showed weak adsorption of $N_2$, and the $N_2$ adsorption capacity at 100 kPa was only 5.8 cc $g^{-1}$. At the same time, the adsorption capacity of bimetal MOF-74 and single metal MOF-74 for $CO_2$ was smaller at 0–10 kPa adsorption partial pressure, but increased with the increase of adsorption partial pressure. In addition, both bimetal MOF-74 and monometallic MOF-74 showed a large adsorption gap between NO and $CO_2$ at lower partial pressure, that is, the adsorption capacity of NO was significantly higher than that of $CO_2$. However, when the adsorption pressure was in the high pressure region, the gap gradually narrowed. At 100 kPa, the adsorption capacities of Co-MOF-74 for NO and $CO_2$ were 149.8 cc $g^{-1}$ and 104.5 cc $g^{-1}$, and

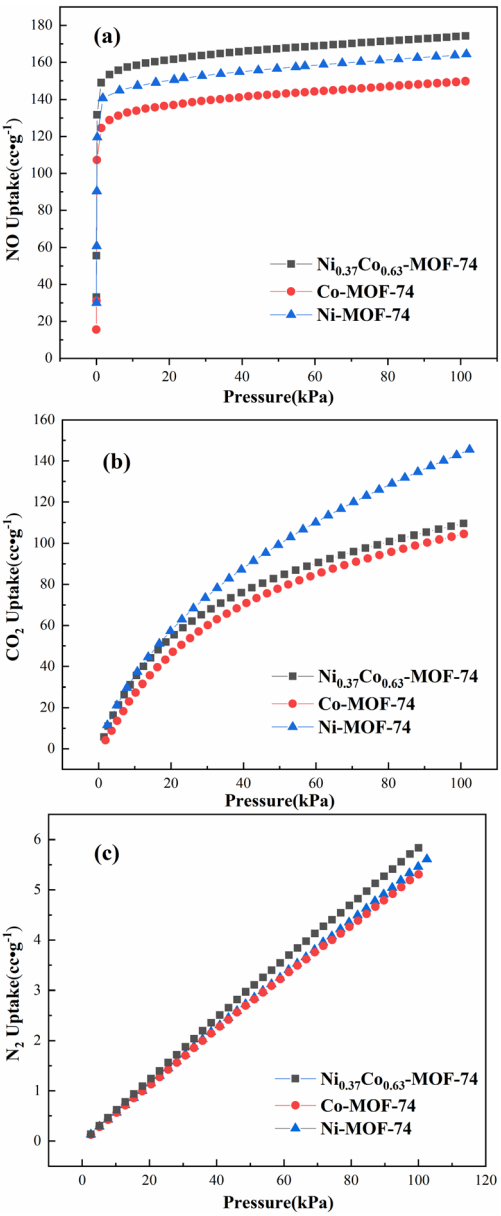


Fig. 5 Gas sorption isotherms of Co-MOF-74, Ni-MOF-74 and $Ni_{0.37}Co_{0.63}$-MOF-74 for NO (a), $CO_2$ (b) and $N_2$ (c) at 298 K.

that of $Ni_{0.37}Co_{0.63}$-MOF-74 were 174.3 cc $g^{-1}$ and 109.5 cc $g^{-1}$ respectively, and yet that of Ni-MOF-74 for NO and $CO_2$ were 164.4 cc $g^{-1}$ and 145.5 cc $g^{-1}$, respectively. Thus it can be seen that the adsorption characteristics of bimetal $Ni_{0.37}Co_{0.63}$-MOF-74 for NO and $CO_2$ were closer to that of Co-MOF-74, but its adsorption capacity for NO was larger, indicating that the Co metal nodes in bimetal samples were beneficial to the selective separation of NO to $CO_2$. Therefore, at 298 K, bimetal $Ni_{0.37}Co_{0.63}$-MOF-74 has a weak adsorption of $N_2$, a stronger adsorption of NO with higher adsorption capacity of NO, and the weaker adsorption in low pressure region and larger adsorption in high pressure region for $CO_2$. This indicated that bimetal $Ni_{0.37}Co_{0.63}$-MOF-74 should have a good prospect in adsorption and separation of NO in flue gas. In order to better illustrate the separation characteristics, it is necessary to simulate the adsorption data in order to compare their selectivity.

The calculation of the IAST adsorption selectivity relied heavily on the simulation of the single component gas adsorption model. The adsorption selectivity was simulated in this paper using the DSLF (Dual Site Langmuir–Freundlich) equation,[23] which was the following specific formula:

$$Q = q_1 \times \frac{b_1 p^c}{1 + b_1 p^c} + q_2 \times \frac{b_2 p^t}{1 + b_2 p^t} \quad (2)$$

where $Q$ was the adsorption selectivity; $q_1$ and $q_2$ were the gas saturated adsorption capacity (mmol $g^{-1}$); $p$ was the pressure at adsorption equilibrium (kPa); $b_1$ and $b_2$ were the correlation coefficients; $c$ and $t$ were the deviation value of ideal surfaces.

Ideal Adsorbed Solution Theory (IAST) is first proposed by Myers and co-worker[24] to predict the selectivity of adsorbents for binary gas mixtures from the adsorption isotherms of single components.[25–27] It is assumed that the mixture of components in the adsorption system is an ideal mixture at a certain diffusion pressure and temperature, where all components follow a rule that the chemical potential energy of the adsorbed phase is equal to that of the gas phase at equilibrium.[25] The performance of gas separation can be predicted more accurately by IAST, such as calculating the selectivity of $NO/CO_2$ adsorption in the flue gas. Adsorption selectivity was defined as below:

$$S_{12} = \frac{x_1}{x_2} \times \frac{y_1}{y_2} \quad (3)$$

Among them, $x_1$ and $x_2$ were the mole fractions of components 1 and 2 on the surface of the adsorbent, and $y_1$ and $y_2$ were the mole fractions of gas components. According to this formula, the adsorption selectivity data of the two gases can be calculated.

The calculated adsorption selectivity of $NO/CO_2$ was shown in Fig. 6. The $NO/CO_2$ adsorption selectivity of $Ni_{0.37}Co_{0.63}$-MOF-74 was about 1.6 and 2.9 times that of Co-MOF-74 and Ni-MOF-74 at low adsorption pressure, and around 1.7 and 2.4 times at high adsorption pressure, respectively, indicating that the introduction of bimetal sites in MOF-74 can improve the adsorption and separation performance of NO. The maximum adsorption selectivity of $Ni_{0.37}Co_{0.63}$-MOF-74 for $NO/CO_2$ can be

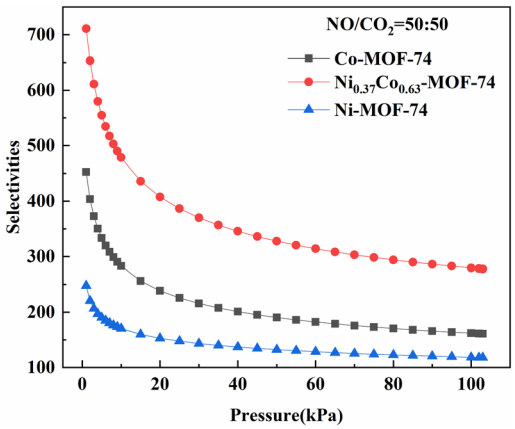


Fig. 6 Adsorption selectivity of Co-MOF-74, Ni-MOF-74 and $Ni_{0.37}Co_{0.63}$-MOF-74 for $NO/CO_2$ predicted by IAST model (298 K).

obtained up to about 710. Under the condition of 0–100 kPa, the adsorption selectivity of $NO/CO_2$ decreased with the increase of pressure, indicating that the sample will give priority to adsorbing NO in the mixed gas at low pressure, and the increase of pressure will decrease the adsorption selectivity of NO and reversely increase the adsorption selectivity of $CO_2$. Therefore, when the material was used in the NO adsorption separation of the mixtures, it should be carried out at a lower adsorption partial pressure, that was to say, the material was more conducive to the adsorption and separation of low concentration nitrogen oxides.

## Stability analysis of material adsorption

The regeneration ability of the adsorption material was very important, and the material saturated with NO adsorption was chosen to be tested again after vacuum degassing treatment at 473 K. The adsorption performance of $Ni_{0.37}Co_{0.63}$-MOF-74 after 5 cycles was shown in Fig. 7 and S3†.

The adsorption capacity of $Ni_{0.37}Co_{0.63}$-MOF-74 for NO were 174.3 cc $g^{-1}$ in the first cycle, 172.4 cc $g^{-1}$ in the second cycle,

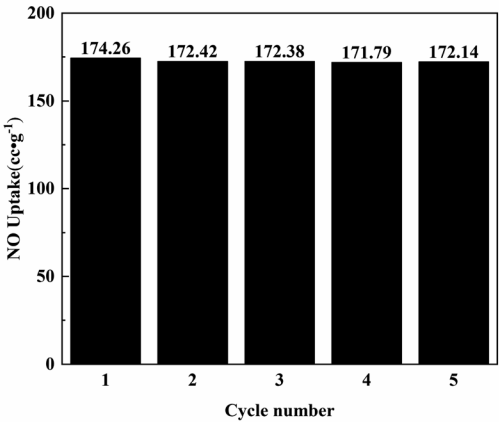


Fig. 7 The adsorption capacity of $Ni_{0.37}Co_{0.63}$-MOF-74 for NO at different regeneration times at 100 kPa.

172.4 cc $g^{-1}$ in the third cycle, 171.8 cc $g^{-1}$ in the fourth cycle, and 172.1 cc $g^{-1}$ in the fifth cycle, respectively. During the cycling process, the NO adsorption capacity of $Ni_{0.37}Co_{0.63}$-MOF-74 hardly decreased, indicating that $Ni_{0.37}Co_{0.63}$-MOF-74 can maintain high stability in the process of NO adsorption and separation, and had an excellent regeneration performance.

The actual flue gas contained a lot of water vapour and was weak acidity due to acidic gases such as nitrogen oxides, so the adsorption separation material should have a certain stability of water resistance and weak acid resistance. Fig. S4† showed the XRD spectra of $Ni_{0.37}Co_{0.63}$-MOF-74 treated with different pH water. It can be seen from the XRD pattern that there was no obvious change in the diffraction peak position of the MOFs material when the sample was immersed in room-temperature pure water (pH = 7) and acid solution (pH = 4) for 72 hours, indicating that the crystal structure of the material has not changed and has certain stability of water and acid resistance. At the same time, the adsorption curve of the sample for NO was basically the same, and the adsorption characteristics and adsorption capacity have no obvious change (Fig. 8), which showed that the material has good water and weak acid resistance stability. These characteristics provided a basis for the adsorption and separation of NO/$CO_2$ in flue gas by bimetal MOFs.

### NO separation in mixed gases (breakthrough curve)

The results of breakthrough experiment in mixed gases were shown in Fig. 9. When the mixed gas flow passed through the reaction tube with $Ni_{0.37}Co_{0.63}$-MOF-74 sample, the mass spectrometer detected a rapid increase in $CO_2$ outlet concentration which reached stability after 40 min, and the $CO_2$ adsorption capacity was around 16.9 cc $g^{-1}$. At the same time, the outlet concentration of NO increased slowly and returned to the initial value after 183 min. At this time, the adsorption reached equilibrium, and the adsorption capacity of NO was about 116.6 cc $g^{-1}$. Calculated by eqn (3), the adsorption selectivity of the sample in the simulated flue gas was about 13.8 for NO/$CO_2$ (seen in Table 2). The adsorption characteristics of the sample in the simulated flue gas were similar to the selective adsorption results calculated by IAST. The synthesized bimetal materials through the introduction of Ni had some potential applications of the adsorption and separation of $NO_x$ in flue gas for resource recovery.

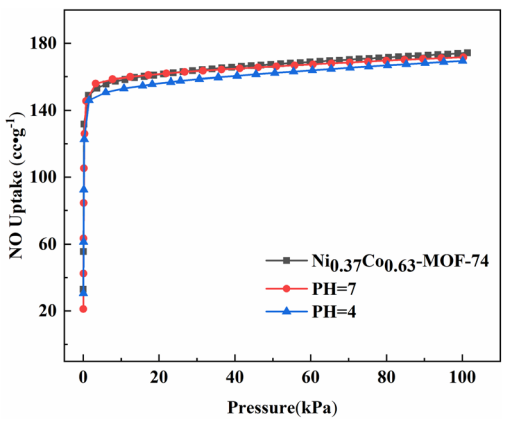


Fig. 8 NO adsorption isotherm of $Ni_{0.37}Co_{0.63}$-MOF-74 after soaking in pH = 4 and pH = 7 for 72 hours.

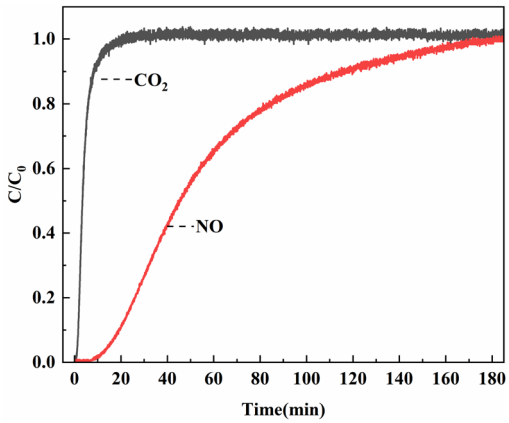


Fig. 9 The breakthrough curve of $Ni_{0.37}Co_{0.63}$-MOF-74.

### Discussion on adsorptive action of NO

The equivalent heat of adsorption was an important parameter to evaluate the interaction between the adsorbent and the adsorbed molecules, and the uniformity of the adsorption surface. It described the heat release by the adsorbent adsorbing a small amount of gas after the quantitative gas had been adsorbed. The isothermal heat of gas adsorption can be calculated by Clausius–Clapeyron equation[28]:

$$Q_{st} = RT_1T_2\frac{\ln(p_2/p_1)}{T_2 - T_1} \quad (4)$$

where $Q_{st}$ was the equivalent heat of adsorption, $R$ was the general gas constant (8.314 J $mol^{-1}$ $K^{-1}$), $T$ was the adsorption temperature and $p$ was the adsorption pressure.

Fig. S6† showed the NO adsorption isotherms on the material at different temperature (273 K and 298 K). The adsorption enthalpy ($Q_{st}$) of the material for each gas component can then be calculated from the Clausius–Clapeyron equation as shown in Fig. 10. The obtained $Q_{st}$ values at zero coverage for NO of Co-MOF-74, Ni-MOF-74 and $Ni_{0.37}Co_{0.63}$-MOF-74 from Fig. 10 to be 34.25 kJ $mmol^{-1}$, 39.98 kJ $mmol^{-1}$ and 41.03 kJ $mmol^{-1}$ respectively. For $CO_2$, the values were 14.76 kJ $mmol^{-1}$, 31.36 kJ $mmol^{-1}$, and 14.29 kJ $mmol^{-1}$ respectively. For $N_2$, the values were 3.77 kJ $mmol^{-1}$, 2.84 kJ $mmol^{-1}$, and 4.8 kJ $mmol^{-1}$ respectively. It can be seen that the NO adsorption enthalpy of bimetal $Ni_{0.37}Co_{0.63}$-MOF-74 was larger than that of single metal Co-MOF-74 and Ni-MOF-74, and by comparison, the adsorption enthalpy of NO was found to be larger than that of $CO_2$ and $N_2$. The adsorption enthalpy directly reflects the strength of the force between the adsorbent and the adsorbent material, it can be concluded that the adsorption strength of Ni-MOF-74, Co-MOF-74 and NiCo-MOF-74 for NO was significantly higher than that for $N_2$ and $CO_2$. This can be coincided with the

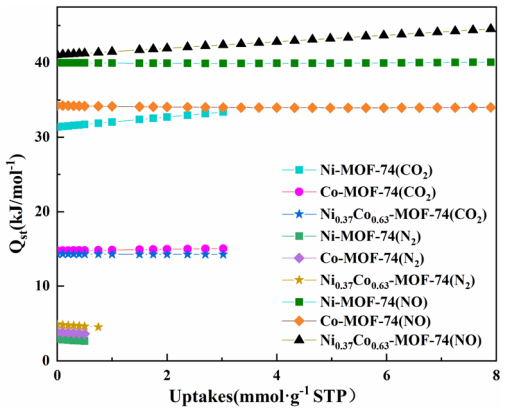


Fig. 10 $CO_2$, $N_2$ and NO adsorption enthalpy of Co-MOF-74, Ni-MOF-74 and $Ni_{0.37}Co_{0.63}$-MOF-74.

Table 2 $Ni_{0.37}Co_{0.63}$-MOF-74 adsorption capacity in mixed atmosphere

| Mixed gas composition | Adsorption capacity (cc $g^{-1}$) | NO adsorption selectivity |
|---|---|---|
| $CO_2$ | 16.9 | 13.8($NO/CO_2$) |
| NO | 116.6 | |

adsorption selectivity results predicted by IAST model (see in Fig. 6) that $Co_{0.37}Ni_{0.63}$-MOF-74 exhibited the most excellent selectivity for NO.

The *in situ* DRIFTS spectra of Ni-MOF-74, Co-MOF-74 and $Ni_{0.37}Co_{0.63}$-MOF-74 after NO adsorption were shown in Fig. 11. After introducing NO for a period of time, Ni-MOF-74 and Co-MOF-74 showed significant adsorption peaks at 1837 $cm^{-1}$ and 1789 $cm^{-1}$ respectively, and the adsorption of NO by bimetal material $Ni_{0.37}Co_{0.63}$-MOF-74 resulted in two adsorption peaks at 1789 $cm^{-1}$ and 1837 $cm^{-1}$. In addition, there was invisible or very weak adsorption peak at around 1038 $cm^{-1}$ assigned to M–$NO_2$ stretch,[29] so the adsorption on the sample was mainly NO adsorbed state. It is generally ascertained that

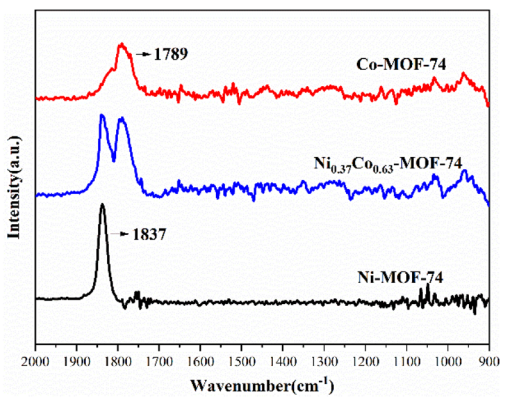


Fig. 11 *In situ* DRIFTS spectra of as-prepared Ni-MOF-74, Co-MOF-74 and $Ni_{0.37}Co_{0.63}$-MOF-74.

NO coordination state through nitrogen atoms with metal centers can be classified into two types of nitrosyl cation ($NO^+$) and nitrosyl anion ($NO^-$), where the M–N–O angle of the nitrosyl cation to the metal is close to 180° (linear), and the that of the nitrosyl anion is generally in the range of 120–140° (bent). In the former case, the electron in the antibonding orbital of NO is donated to the metal atom forming σ-bond, a large amount of charge will be transferred to the metal, while in the latter case, a π-bond is then provided by the donation of electrons from metal to the antibonding orbital of nitric oxide, the charge will be transferred in the opposite direction with a large amount of charge transferred to NO.[30] The adsorption peaks of NO adsorbed by Ni-MOF-74, Co-MOF-74 and $Ni_{0.37}Co_{0.63}$-MOF-74 at 1789 $cm^{-1}$ and 1837 $cm^{-1}$ can be attributed to linear coordination adsorption state of Co(II)···NO and Ni(II)···NO, no bending coordination adsorption was formed,[31] showing a strong interaction of the adsorbed NO with the metal sites of the samples.[32] The IR spectroscopy results showed that NO adsorption occurred at both Ni and Co metal centers on $Ni_{0.37}Co_{0.63}$-MOF-74, and the electric charge on NO was transferred to the metal to form σ-bond linear coordination adsorption. Because the NO adsorption enthalpy of bimetal $Ni_{0.37}Co_{0.63}$-MOF-74 was larger than that of single metal Co-MOF-74 and was consistent with the adsorption capacity of NO, there should be a certain synergistic effect between the two metal centers.[22]

The adsorption of NO, $CO_2$ and $N_2$ was investigated in detail by selecting $Ni_{0.37}Co_{0.63}$-MOF-74, Co-MOF-74 and Ni-MOF-74. The adsorption of NO was found to be better than that of $CO_2$ and $N_2$. This difference in adsorption manifested on the same material depended on the nature of the adsorbed gas molecules to a large extent. Previous studies were shown that the large quadrupole distance of $CO_2$ leads to a lateral force between the $CO_2$ molecule and the oxygen atom of the ligand, and this geometric configuration reduces the adsorption properties of $CO_2$ to some extent.[33] The shorter NO and $N_2$ molecules maintained linear adsorption, while the interaction between metal sites and $N_2$ was not so strong, and was more affected by electrostatic force.[34] The interaction between MOF-74 and NO was stronger by activating exposed metal sites and pore structure. At the same time, the synergistic effect between different metal sites increased the adsorption energy of bimetal $Ni_{0.37}Co_{0.63}$-MOF-74 samples compared with single metal, and the adsorption of NO can further enhance the adsorption properties of materials through dispersion force.[35]

## Conclusions

The bimetal node microporous NiCo-MOF-74 synthesized by solvothermal method had the surface morphology as rod-like crystal and typical MOF-74 crystal structure. Ni and Co elements were uniformly distributed in the crystal, and its thermal stability can withstand 320 °C.

$Ni_{0.37}Co_{0.63}$-MOF-74 showed weak adsorption to $N_2$ at 298 K, and its NO adsorption capacity reached 174.3 cc $g^{-1}$ at 100 kPa, which was higher than that of single metal MOF-74. Although $Ni_{0.37}Co_{0.63}$-MOF-74 had a small adsorption capacity for $CO_2$

and can obtain $NO/CO_2$ adsorption selectivity up to about 710 at low adsorption pressure, but its $CO_2$ adsorption capacity increased with the increase of adsorption partial pressure and led to the decrease of $NO/CO_2$ adsorption selectivity. The adsorption and separation characteristics of bimetal $Ni_{0.37}Co_{0.63}$-MOF-74 for NO and $CO_2$ were closer to that of Co-MOF-74. In comparison, the $NO/CO_2$ adsorption selectivity of $Ni_{0.37}Co_{0.63}$-MOF-74 was 1.6 and 2.9 times that of Co-MOF-74 and Ni-MOF-74 at low adsorption pressure, and 1.7 and 2.4 times at high adsorption pressure, respectively.

NO adsorption occurred in both Ni and Co metal centers on $Ni_{0.37}Co_{0.63}$-MOF-74, and the adsorptive modes were linear adsorption of Co(II)···NO and Ni(II)···NO. At the same time, the NO adsorption enthalpy of bimetal $Ni_{0.37}Co_{0.63}$-MOF-74 was larger than that of single metal Co-MOF-74, and all three materials have a larger NO adsorption enthalpy than that of $CO_2$ and $N_2$. The experiment of water and acid resistance showed that $Ni_{0.37}Co_{0.63}$-MOF-74 had good stability of water resistance and weak acid resistance, and still had stable NO adsorption performance after 5 adsorption–desorption cycles. Meanwhile, in the breakthrough experiments, the adsorption separation ratio of $NO/CO_2$ in mixed gas can reach about 13.8 with a high adsorption separation effect, indicating that $Ni_{0.37}Co_{0.63}$-MOF-74 was suitable for the adsorption and separation of NO in flue gas.

## Conflicts of interest

The authors confirm that this article content has no conflict of interest.

## Acknowledgements

FT thanks the financial support of Guangxi Science Research and Technology Development Project of China (Grant No. AA18118010).

## Notes and references

1 K. Skalska, J. S. Miller and S. Ledakowicz, Trends in $NO_x$ abatement: a review, *Sci. Total Environ.*, 2010, **19**, 3976–3989.
2 M. Y. Chen, M. M. Zhao, F. S. Tang, *et al.*, Effect of Ce doping into $V_2O_5$-$WO_3/TiO_2$ catalysts on the selective catalytic reduction of $NO_x$ by $NH_3$, *J. Rare Earths*, 2017, **12**, 1206–1215.
3 R. B. Lin, Z. J. Zhang and B. L. Chen, Achieving High Performance Metal–Organic Framework Materials through Pore Engineering, *Acc. Chem. Res.*, 2021, **17**, 3362–3376.
4 R. B. Lin, S. C. Xiang, W. Zhou, *et al.*, Microporous Metal–Organic Framework Materials for Gas Separation, *Chem*, 2020, **2**, 337–363.
5 B. Li, H. Wen, Y. Yu, *et al.*, Nanospace within metal–organic frameworks for gas storage and separation, *Mater. Today Nano*, 2018, **2**, 21–49.
6 S. C. Li, Y. Zhai, X. X. Wei, *et al.*, Catalytic Performance of MIL-88B(V) and MIL-101(V) MOFs for the Selective Catalytic Reduction of NO with $NH_3$, *ChemCatChem*, 2021, **3**, 940–951.
7 R. B. Lin, Y. He, P. Li, *et al.*, Multifunctional Porous Hydrogen-Bonded Organic Framework Materials, *Chem. Soc. Rev.*, 2019, **5**, 1362–1389.
8 D. Yu, A. O. Yazaydin, J. R. Lane, *et al.*, A combined experimental and quantum chemical study of $CO_2$ adsorption in the metal–organic framework CPO-27 with different metals, *Chem. Sci.*, 2013, **4**(9), 3544–3556.
9 T. L. Easun, F. Moreau, Y. Yan, *et al.*, Structural and dynamic studies of substrate binding in porous metal–organic frameworks, *Chem. Soc. Rev.*, 2017, **1**, 239–274.
10 P. D. C. Dietzel, V. Besikiotis and R. Blom, Application of metal–organic frameworks with coordinatively unsaturated metal sites in storage and separation of methane and carbon dioxide, *J. Mater. Chem.*, 2009, **39**, 7362–7370.
11 T. G. Glover, G. W. Peterson, B. J. Schindler, *et al.*, MOF-74 building unit has a direct impact on toxic gas adsorption, *Chem. Eng. Sci.*, 2011, **2**, 163–170.
12 N. L. Rosi, J. Kim, M. Eddaoudi, *et al.*, Rod packings and metal–organic frameworks constructed from rod-shaped secondary building units, *J. Am. Chem. Soc.*, 2005, **5**, 1504–1518.
13 L. J. Wang, H. X. Deng, H. Furukawa, *et al.*, Synthesis and characterization of metal–organic framework-74 containing 2, 4, 6, 8, and 10 different metals, *Inorg. Chem.*, 2014, **12**, 5881–5883.
14 N. J. Hinks, A. C. Mckinlay, X. Bo, *et al.*, Metal organic frameworks as NO delivery materials for biological applications, *Microporous Mesoporous Mater.*, 2010, **3**, 330–334.
15 A. C. Mckinlay, X. Bo, D. S. Wragg, *et al.*, Exceptional behavior over the whole adsorption-storage-delivery cycle for NO in porous metal organic frameworks, *J. Am. Chem. Soc.*, 2008, **31**, 10440–10444.
16 J. A. Botas, G. Calleja, M. Sanchez-Sanchez, *et al.*, Effect of Zn/Co ratio in MOF-74 type materials containing exposed metal sites on their hydrogen adsorption behaviour and on their band gap energy, *Int. J. Hydrogen Energy*, 2011, **17**, 10834–10844.
17 D. Cattaneo, S. J. Warrender, M. J. Duncan, *et al.*, Tuning the nitric oxide release from CPO-27 MOFs, *RSC Adv.*, 2016, **17**, 14059–14067.
18 H. Furukawa, K. E. Cordova, M. O'Keeffe, *et al.*, The chemistry and applications of metal–organic frameworks, *Science*, 2013, **6149**, 1230444.
19 S. R. Chen, M. Xue, Y. G. Li, *et al.*, Rational design and synthesis of $Ni_xCo_{3-x}O_4$ nanoparticles derived from multivariate MOF-74 for supercapacitors, *J. Mater. Chem. A*, 2015, **40**, 20145–20152.
20 J. Liu, J. Zheng, D. Barpaga, *et al.*, A Tunable Bimetallic MOF-74 for Adsorption Chiller Applications, *Eur. J. Inorg. Chem.*, 2018, **7**, 885–889.
21 Y. B. Zhang, H. Furukawa, N. Ko, *et al.*, Introduction of Functionality, Selection of Topology, and Enhancement of Gas Adsorption in Multivariate Metal–Organic Framework-177, *J. Am. Chem. Soc.*, 2015, **7**, 2641–2650.

22 J. A. Villajos, G. Orcajo, C. Martos, *et al.*, Co/Ni mixed-metal sited MOF-74 material as hydrogen adsorbent, *Int. J. Hydrogen Energy*, 2015, **15**, 5346–5352.
23 X. Wu, Z. Bao, B. Yuan, *et al.*, Microwave synthesis and characterization of MOF-74 (M = Ni, Mg) for gas separation, *Microporous Mesoporous Mater.*, 2013, **180**, 114–122.
24 A. L. Myers and J. M. Prausnitz, Thermodynamics of mixed-gas adsorption, *AIChE J.*, 1965, **1**, 121–127.
25 W. Huang, X. Zhou, Q. Xia, *et al.*, Preparation and Adsorption Performance of GrO@Cu-BTC for Separation of $CO_2/CH_4$, *Ind. Eng. Chem. Res.*, 2014, **27**, 11176–11184.
26 Z. J. Zhang, S. C. Xiang and B. L. Chen, Microporous metal–organic frameworks for acetylene storage and separation, *CrystEngComm*, 2011, **20**, 5983–5992.
27 R. Krishna and J. M. van Baten, *In silico* screening of metal–organic frameworks in separation applications, *Phys. Chem. Chem. Phys.*, 2011, **22**, 10593–10616.
28 A. Nuhnen and C. Janiak, A practical guide to calculate the isosteric heat/enthalpy of adsorption *via* adsorption isotherms in metal–organic frameworks, MOFs, *Dalton Trans.*, 2020, **30**, 10295–10307.
29 D. F. S. Gallis, D. J. Vogel, G. A. Vincent, *et al.*, $NO_x$ adsorption and optical detection in rare earth metal–organic frameworks, *ACS Appl. Mater. Interfaces*, 2019, **46**, 43270–43277.
30 P. C Ford and I. M Lorkovic, Mechanistic aspects of the reactions of nitric oxide with transition-metal complexes, *Chem. Rev.*, 2002, **102**(4), 993–1018.
31 F. Bonino, S. Chavan, J. G. Vitillo, *et al.*, Local Structure of CPO-27-Ni Metalorganic Framework upon Dehydration and Coordination of NO, *Chem. Mater.*, 2008, **15**, 4957–4968.
32 M. Mihaylov and K. Hadjiivanov, FTIR Study of CO and NO Adsorption and Coadsorption on Ni-ZSM-5 and $Ni/SiO_2$, *Langmuir*, 2002, **11**, 4376–4383.
33 J. R. Li, R. J. Kuppler and H. C. Zhou, Selective gas adsorption and separation in metal–organic frameworks, *Chem. Soc. Rev.*, 2009, **5**, 1477–1504.
34 L. Valenzano, J. G. Vitillo, S. Chavan, *et al.*, Structure–activity relationships of simple molecules adsorbed on CPO-27-Ni metal–organic framework: *in situ* experiments *vs.* theory, *Catal. Today*, 2012, **1**, 67–79.
35 L. Valenzano, B. Civalleri, S. Chavan, *et al.*, Computational and Experimental Studies on the Adsorption of CO, $N_2$, and $CO_2$ on Mg-MOF-74, *J. Phys. Chem. C*, 2010, **25**, 11185–11191.